



## Barnett field, rotational Doppler effect, and Berry phase studied by nuclear quadrupole resonance with rotation

H. Chudo <sup>1,\*</sup> M. Matsuo <sup>2,1,3</sup> S. Maekawa,<sup>1,2,3</sup> and E. Saitoh<sup>1,4,5,6</sup>

<sup>1</sup>*Advanced Science Research Center, Japan Atomic Energy Agency, Tokai, Ibaraki 319-1195, Japan*

<sup>2</sup>*Kavli Institute for Theoretical Sciences, University of Chinese Academy of Sciences, 19 Yuquan Road, Beijing 100049, People's Republic of China*

<sup>3</sup>*Riken Center for Emergent Matter Science, Wako 351-0198, Japan*

<sup>4</sup>*Department of Applied Physics, The University of Tokyo, Hongo, Bunkyo-ku, Tokyo 113-8656, Japan*

<sup>5</sup>*Institute for AI and Beyond, The University of Tokyo, Tokyo 113-8656, Japan*

<sup>6</sup>*Advanced Institute for Materials Research, Tohoku University, Sendai 980-8577, Japan*



(Received 15 December 2020; accepted 26 April 2021; published 24 May 2021)

We report the observation of the Barnett field, rotational Doppler effect, and Berry phase using the rotating nuclear quadrupole resonance (NQR) method. We have developed coil-spinning techniques that enable us to systematically study the effects of rotation in setups involving rotation of the signal detector, rotation of the sample, and simultaneous rotation of both the signal detector and sample. Applying these setups to NQR measurements, we observe NQR line splittings in which the spectral structures are clearly distinct among the setups. By analyzing these structures, we clarify the origin of the NQR line splittings and discuss the relationship between the rotational Doppler effect, Barnett field effect, and Berry phase in terms of the rotational degrees of freedom, such as the relative rotation and the sample rotation itself, and the observation frame of reference. We also provide clear evidence of the difference between the rotational Doppler effect and the Barnett field and the equivalence of the Barnett field and the Berry phase.

DOI: [10.1103/PhysRevB.103.174308](https://doi.org/10.1103/PhysRevB.103.174308)

### I. INTRODUCTION

The interaction between the spin of an electron and mechanical rotation has played a crucial role in the development of quantum physics. A century ago, the first experimental proof that an electron spin has angular momentum was provided by experiments on the Barnett effect and Einstein–de Haas effect [1–4]. These studies experimentally determined the value of the  $g$  factor of an electron to be  $\sim 2$  prior to the establishment of modern quantum physics. The Einstein–de Haas effect has been exploited to determine the  $g$  factors of electrons in various materials and the orbital component of the magnetic moment [5,6].

Alongside recent advances in physics and technology, the interaction between the spin of an electron and mechanical rotation has once again attracted attention at the frontier of contemporary physics, especially in terms of spintronics and the physics of quantum geometric phases [7,8], such as Berry phases. The Berry phase provides us with a new way to deal with a cyclic time-dependent Hamiltonian and has also been discovered in mechanical systems [9–12]. Concurrently, in the field of spintronics, the Einstein–de Haas effect has been exploited to mechanically manipulate microscale devices such as cantilevers [13,14] and paddles [15,16] fabricated by using nanotechnology. The Barnett effect has also been used to generate a spin current from mechanical motion such as fluid

flows [17–20] and surface acoustic waves [21,22] and to detect the angular momentum compensation point [23,24].

The Barnett effect has also been observed in nuclear spin systems [25–28]. The origin of the Barnett effect is spin-rotation coupling [29], which is formulated from the relativistic quantum theory [19,30,31]. The spin-rotation coupling is interpreted as an effective magnetic field, referred to as the Barnett field  $B_\Omega = \Omega/\gamma$ , where  $\Omega$  is the angular velocity of a rotating sample and  $\gamma$  is the gyromagnetic ratio [29,32,33]. As the Barnett field is an inertial field analog of the Coriolis force in a rotating frame of reference, an observer must be in the same rotating frame of reference as the rotating sample to observe the inertial force.

We have observed the Barnett field acting on nuclei by using the specially designed NMR circuit depicted in Fig. 1(a), which enables us to detect NMR signals in the same rotating frame as a rotating sample [25]. The circuit consists of a sample coil for detecting the NMR signal and a coupling coil for transmitting the NMR signal from the rotating frame to the laboratory frame. Using this circuit, we can observe the NMR shift by a frequency of  $\Omega/2\pi$ , which corresponds to the rotational frequency, owing to the Barnett field. Furthermore, using a similar circuit and a stationary sample, we can observe the rotational Doppler effect [26]. This effect also causes the NMR frequency to shift by the same frequency  $\Omega/2\pi$  corresponding to the rotational frequency. Furthermore, upon rotating only the sample, the two effects cancel each other out, resulting in no NMR shift [26].

However, because of the equality of the NMR shift arising from the Barnett field and the rotational Doppler effect, Jeener

\*chudo.hiroyuki@jaea.go.jp

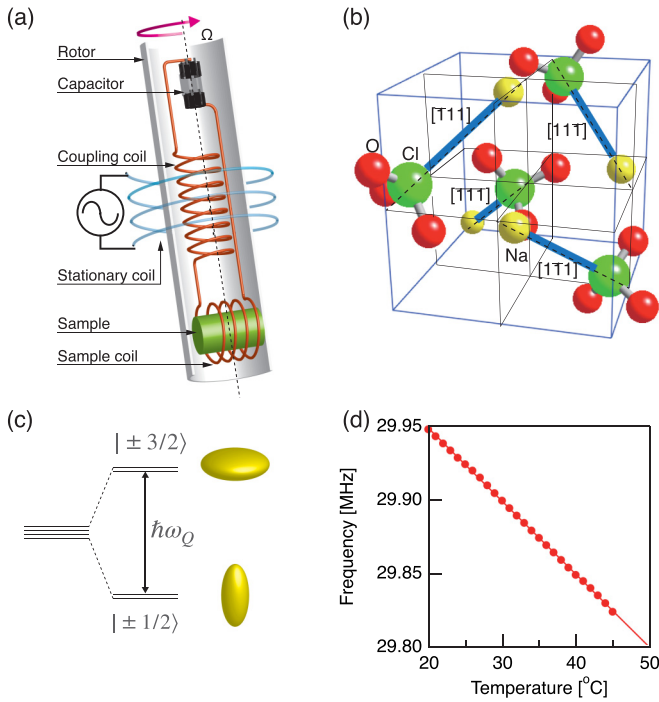


FIG. 1. (a) Typical hardware for the present rotating NQR measurements. (b) Unit cell of  $\text{NaClO}_3$ . (c) Schematic illustration of the energy level splitting due to the quadrupole interaction for nuclear spin  $J = 3/2$ . (d) Temperature dependence of the NQR frequency  $\omega_Q/2\pi$ .

criticized that the NMR shifts observed in the above two setups, namely, with simultaneous rotation of both the sample and the sample coil and rotation of only the sample coil, may be explained solely by the sample coil rotation and thus that rotating the sample is not essential; he denied the existence of the Barnett field as an unnecessary hypothesis [34]. In the NMR community, nuclear spins in a rotating material have been considered to be decoupled from the rotational motion of the material, and thus, the Barnett field has not been accepted as the inertial force in a rotating frame of reference [28,34,35]. On the other hand, the Berry phase has been studied using NMR and nuclear quadrupole resonance (NQR) and has been accepted in the NMR community, even though both the Berry phase and the Barnett field are gauge fields in a certain coordinate frame of reference [11,36].

In this paper, we provide explicit experimental evidence of the difference between the Barnett field and the rotational Doppler effect by using a rotating NQR method. The NQR line split into two lines upon rotation of only the sample coil, while the NQR line split into three lines upon simultaneous rotation of both the sample and the sample coil. These findings indicate that the nuclear spin in the rotating material couples with the external rotation and is affected by the inertial electromagnetic force, that is, the Barnett field. In addition, we also demonstrate the equivalence of the Berry phase and the Barnett field as a gauge field in a certain coordinate frame of reference. We formulate the Barnett field, rotational Doppler effect, and Berry phase in a unified way and straighten out the relation between them.

## II. EXPERIMENTAL METHODS

We chose a single crystal of a sodium chlorate ( $\text{NaClO}_3$ ) as the sample for measurements because the linewidth in the  $^{35}\text{Cl}$  NQR spectrum of  $\text{NaClO}_3$  is sufficiently narrow to permit the effects of rotation to be evaluated using our current experimental equipment (produced by JEOL), which has a maximum rotational frequency of 22 kHz. Figure 1(b) shows the crystal structure of  $\text{NaClO}_3$ . The unit cell contains four  $\text{NaClO}_3$  molecules. The principal axis of the electric field gradient (EFG) at the Cl sites in the molecule is axially symmetric along the bond joining Na and Cl atoms. In the crystal, the principal axis of the EFG is directed along  $\langle 111 \rangle$ .

As the nuclear spin of  $^{35}\text{Cl}$  is  $J = 3/2$  and has a quadrupole moment, its energy levels split into two degenerate levels in the uniaxial EFG as follows:

$$\mathcal{H}_Q = \frac{e^2qQ}{4J(2J-1)}(3J_z^2 - J^2) = A \begin{pmatrix} 3 & & & \\ & -3 & & \\ & & -3 & \\ & & & 3 \end{pmatrix}, \quad (1)$$

where  $\mathcal{H}_Q$  is the quadrupole Hamiltonian and  $A$  is defined as  $e^2qQ/4J(2J-1)$ . The spin states of  $k = 3/2, -3/2$  and  $k = 1/2, -1/2$  degenerate as shown in Fig. 1(c). Transitions are possible between  $3/2 \leftrightarrow 1/2$  and  $-3/2 \leftrightarrow -1/2$ . Then, the NQR frequency  $\omega_Q/2\pi$  can be expressed as  $6A/h$  and is 29.898 MHz at 30 °C. The gyromagnetic ratio  $\gamma/2\pi$ , quadrupole moment  $Q$ , and natural abundance of  $^{35}\text{Cl}$  are +4.172 MHz/T,  $-8.2 \times 10^{-26}$  cm<sup>2</sup>, and 75.77%, respectively. The temperature dependence of the NQR frequency is 4.95 kHz/K at around room temperature, as shown in Fig. 1(d). Thus, we carefully controlled the temperature within 0.01 K during the measurements.

The single crystal was grown by slow evaporation from a saturated aqueous solution of  $\text{NaClO}_3$ . The crystal axis was determined by x-ray diffraction. The edge of the as-grown single crystal corresponded to the  $\langle 100 \rangle$  direction. The rotating axis was also along the  $\langle 100 \rangle$  direction. Under these conditions, the four Cl sites in the unit cell were equivalent, and the angle  $\theta$  between the principal axis of the EFG and the rotation axis could be expressed as  $\cos \theta = \sqrt{1/3}$ .

Figure 1(a) shows the hardware used for the present measurements. The coil rotation was realized using a specially arranged tuning circuit positioned in a high-speed rotor, which was installed inside a stationary coil and isolated mechanically from the outer circuit. Electromagnetic coupling between the outer and inner circuits was realized by the mutual induction between the stationary coil and coupling coil. Both coils were parallel to the rotation axis. In this configuration, the rotational Doppler effect does not occur between the stationary coil and the coupling coil, as shown in the following. Additional details regarding the hardware are provided in Refs. [25,26]. All of the experiments were performed under zero magnetic field. The temperature during the NQR measurements was maintained at 30 °C by controlling the temperature of the air flow that drove the high-speed rotor.

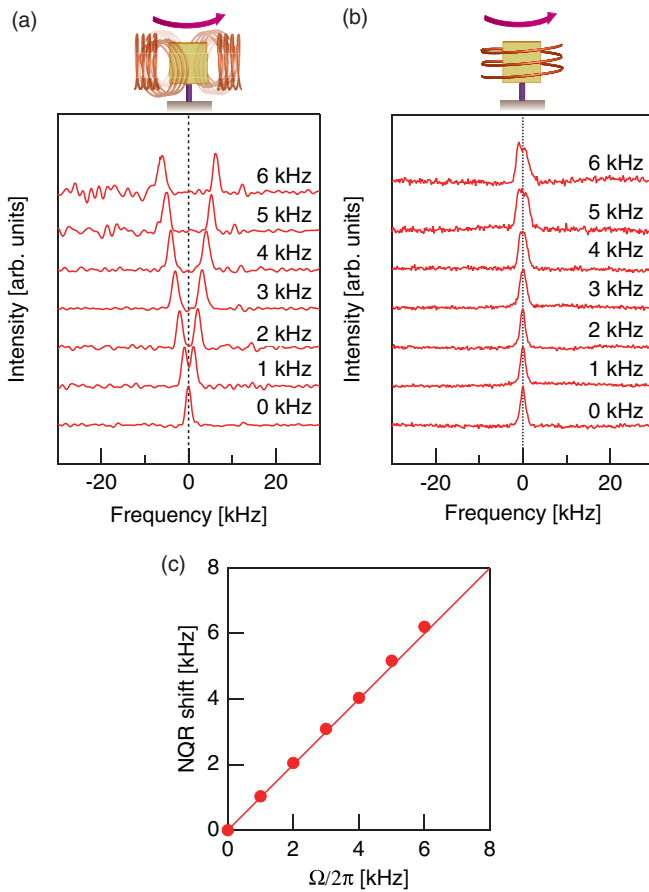


FIG. 2. (a) and (b)  $^{35}\text{Cl}$  NQR spectra at various values of the rotational frequency (0–6 kHz) obtained under only sample coil rotation with the coil (a) perpendicular and (b) parallel to the rotation axis. The origin of the horizontal axis is the center of the NQR spectra at  $\Omega = 0$ , that is,  $\omega_Q/2\pi$ . (c) Rotational frequency dependence of the NQR shift shown in (a). The solid line is intended to serve as a guide to the eye. The slope of the line is 1.

### III. EXPERIMENTAL RESULTS

#### A. Only coil rotation

In Figs. 2(a) and 2(b), we show the  $^{35}\text{Cl}$  NQR spectra measured under only sample coil rotation. In this setup, the sample was fixed in the laboratory frame of reference, and no external field was applied to the sample. In spite of this, the NQR spectrum splits into two lines with equal intensity, as shown in Fig. 2(a), and each shift was  $\pm\Omega/2\pi$ , as shown in Fig. 2(c). This splitting was caused by the relative rotation between the sample and the sample coil because of the lack of an external field acting on the sample. Thus, we call this the rotational Doppler effect.

In the case of the longitudinal coil, as shown in Fig. 2(b), in contrast, no line splitting was observed at rotational frequencies up to 6 kHz. This result indicates that the rotational Doppler effect does not appear in the configuration with the coil axis parallel to the rotation axis. The line broadening observed at rotational frequency above 4 kHz was caused by the temperature distribution in the sample due to the friction with the air. This temperature distribution was estimated to be  $\pm 0.02$  K over the sample.

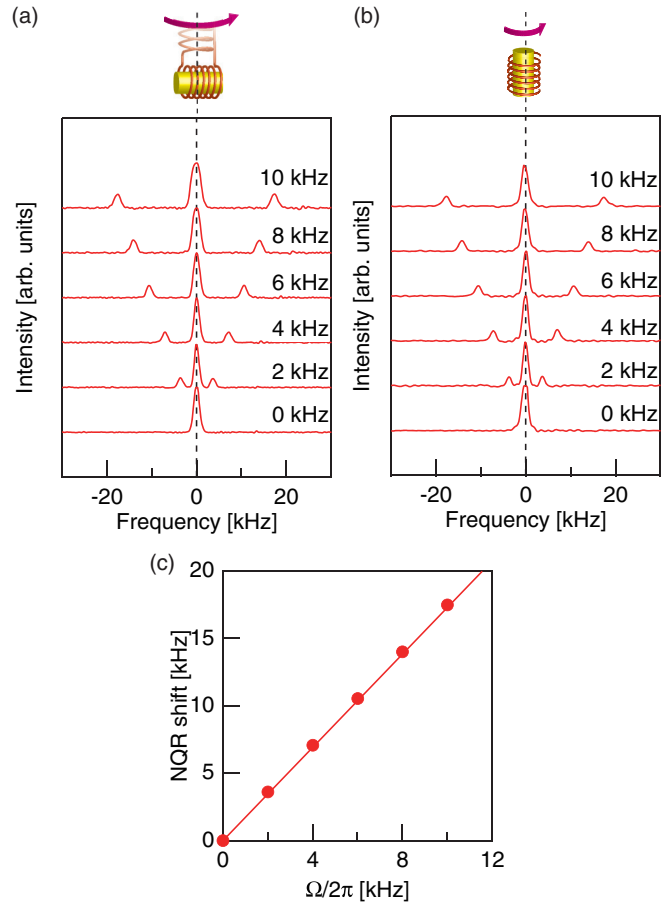


FIG. 3. (a) and (b)  $^{35}\text{Cl}$  NQR spectra at various values of the rotational frequency (0–10 kHz) obtained under simultaneous sample and sample coil rotation with the coil (a) perpendicular and (b) parallel to the rotation axis. The origin of the horizontal axis is the center of the NQR spectra obtained at  $\Omega = 0$ , i.e.,  $\omega_Q/2\pi$ . (c) Rotational frequency dependence of the shift of the satellite lines. The solid line is intended to serve as a guide to the eye. The slope of the line is  $\sqrt{3}$ .

#### B. Simultaneous sample and sample coil rotation

In Figs. 3(a) and 3(b), we present the  $^{35}\text{Cl}$  NQR spectra obtained under simultaneous rotation of both the sample and sample coil for the transverse coil and the longitudinal coil, respectively. For both the transverse and longitudinal coil rotations, we obtained the same NQR spectra. These NQR spectra are different from those in Figs. 2(a) and 2(b) that were obtained under only coil rotation. The single line at  $\Omega = 0$  splits into three lines under the rotation, which were separated by  $\sqrt{3}\Omega/2\pi$ , as shown in Fig. 3(c). In both cases, there was no relative rotation between the sample and sample coil, that is, no rotational Doppler effect. Therefore, the line splitting was caused by the Barnett field emerging along the rotation axis owing to the sample rotation.

#### C. Only sample rotation

In Fig. 4, we show the  $^{35}\text{Cl}$  NQR spectra obtained under only sample rotation. This setup involves both sample rotation itself and the relative rotation. Figure 4(a) presents the NQR spectra obtained for the transverse coil in the stationary frame

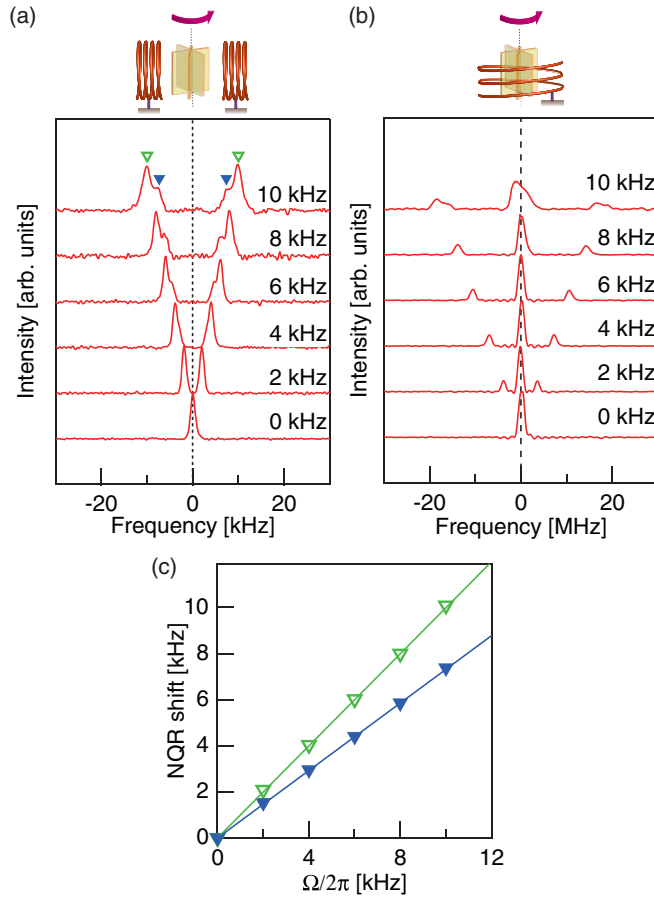


FIG. 4. (a) and (b)  $^{35}\text{Cl}$  NQR spectra at various values of the rotational frequency (0–10 kHz) obtained under only sample rotation with the coil (a) perpendicular and (b) parallel to the rotation axis. The origin of the horizontal axis is the center of the NQR spectra obtained at  $\Omega = 0$ , that is,  $\omega_Q$ . (c) Rotational frequency dependence of the shifts presented in (a). The solid lines are intended to serve as a guide to the eye. The slopes of the green and blue lines are 1 and  $\sqrt{3} - 1$ , respectively.

of reference. The NQR line splits into two, and each of the resulting lines has a shoulder, as indicated by the open green triangles and solid blue triangles, respectively. In contrast, as shown in Fig. 4(b), for the longitudinal coil the NQR spectra split into three lines, and the separation of the lines was proportional to  $\sqrt{3}\Omega/2\pi$ . The NQR spectra obtained for the longitudinal coil were identical to those shown in Figs. 3(a) and 3(b). The origin of the difference between the NQR spectra shown in Fig. 4(a) and those shown in Figs. 4(b), 3(a), and 3(b) was the occurrence of the rotational Doppler effect in the former case. The rotational frequency dependence of these four shifts in Fig. 4(a) is summarized in Fig. 4(c). The dependence of the peak and shoulder frequencies on rotational frequency is proportional to  $\Omega/2\pi$  and  $(\sqrt{3} - 1)\Omega/2\pi$ , respectively.

## IV. THEORETICAL CALCULATIONS

### A. Only coil rotation

We formulate the NQR spectra shown in Figs. 2(a) and 2(b) in the following. The time evolution of the nuclear spin states

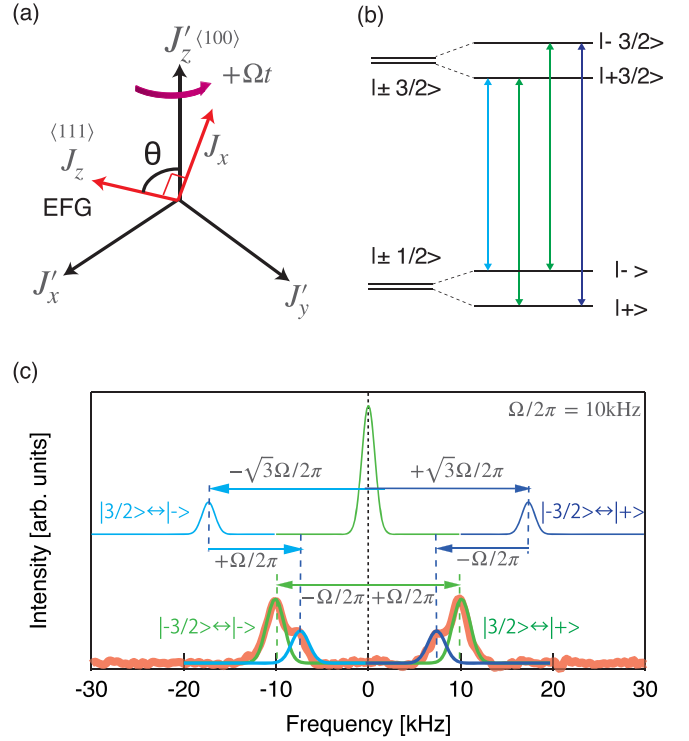


FIG. 5. (a) Definition of the coordinate axes for the calculations, the direction of rotation, and the principal axis of the EFG. (b) Schematic illustration of the energy state splitting due to the Zeeman interaction of the Barnett field in addition to the quadrupole interaction. (c) The green and light and dark blue curves are the simulations using Eqs. (17a)–(17d) or Eqs. (32a)–(32d) and Eqs. (24a)–(24d) or (33a)–(33d) for the upper and lower NQR spectra, respectively. The red curve in (c) is the experimental data shown in Fig. 4(a) with a rotational frequency of 10 kHz.

can be written as

$$|k; t\rangle = e^{\int_0^t dt' \mathcal{H}_Q / i\hbar} |k; 0\rangle, \quad (2)$$

where  $k$  denotes  $3/2$ ,  $1/2$ ,  $-1/2$ , or  $-3/2$ . We define the operator for the rotational Doppler effect as follows:

$$e^{-i\theta J'_y} e^{-i\Omega t J'_z} J'_j e^{i\Omega t J'_z} e^{i\theta J'_y}, \quad (3)$$

where  $J'_j$  denotes  $J'_z$  or  $J'_\pm$ .  $J'_z$  and  $J'_\pm$  are spin operators parallel and perpendicular to the rotation axis, respectively.  $e^{\pm i\theta J'_y}$  expresses the rotation of the spin state  $|k\rangle$  around the  $y$  axis in terms of  $\theta$ , which is the angle between the coil rotation axis and the principal axis of the EFG in the crystal and is expressed as  $\cos \theta = \sqrt{1/3}$ , as shown in Fig. 5(a).  $e^{-i\Omega t J'_z} J'_j e^{i\Omega t J'_z}$  represents the rotation of the observable  $J'_j$  along the  $z$  axis with a frequency of  $\Omega/2\pi$ . This operator corresponds to the rotation with the sample coil as the observer. The general formula for the expected value of the time-dependent spin state for a rotational Doppler effect can be expressed as

$$\begin{aligned} & \langle k'; t | e^{-i\theta J'_y} e^{-i\Omega t J'_z} J'_j e^{i\Omega t J'_z} e^{i\theta J'_y} | k; t \rangle \\ &= \langle k'; 0 | e^{-\int_0^t dt' \mathcal{H}_Q / i\hbar} e^{-i\theta J'_y} e^{-i\Omega t J'_z} J'_j e^{i\Omega t J'_z} e^{i\theta J'_y} \\ & \quad \times e^{\int_0^t dt' \mathcal{H}_Q / i\hbar} | k; 0 \rangle \\ &= e^{-(E_0^{k'} - E_0^k)t / i\hbar} \langle k'; 0 | e^{-i\theta J'_y} e^{-i\Omega t J'_z} J'_j e^{i\Omega t J'_z} e^{i\theta J'_y} | k; 0 \rangle, \quad (4) \end{aligned}$$



where  $E_Q^k$  is the eigenvalue of  $\mathcal{H}_Q$  for spin state  $k$ .

In the case of a longitudinal coil [Fig. 2(b)], we define the observable  $J_j'$  to be  $J_z'$ . Then, the observable can be calculated as follows:

$$e^{-i\theta J_y'} e^{-i\Omega t J_z'} J_z' e^{i\Omega t J_z'} e^{i\theta J_y'} = e^{-i\theta J_y'} J_z' e^{i\theta J_y'}. \quad (5)$$

The expected values can be calculated as

$$\begin{aligned} \langle 3/2; t | e^{-i\theta J_y'} e^{-i\Omega t J_z'} J_z' e^{i\Omega t J_z'} e^{i\theta J_y'} | 1/2; t \rangle \\ = e^{i\omega_Q t} \langle 3/2; 0 | e^{-i\theta J_y'} J_z' e^{i\theta J_y'} | 1/2; 0 \rangle, \end{aligned} \quad (6a)$$

$$\begin{aligned} \langle -3/2; t | e^{-i\theta J_y'} e^{-i\Omega t J_z'} J_z' e^{i\Omega t J_z'} e^{i\theta J_y'} | -1/2; t \rangle \\ = e^{i\omega_Q t} \langle -3/2; 0 | e^{-i\theta J_y'} J_z' e^{i\theta J_y'} | -1/2; 0 \rangle. \end{aligned} \quad (6b)$$

This result indicates that, in the case of the longitudinal coil rotation, the expected value of a spin state rotates with frequency  $\omega_Q/2\pi$  and the NQR signal does not exhibit any shift. This result is consistent with the NQR spectra, as shown in Fig. 2(b).

On the other hand, in the case of transverse coil rotation [Fig. 2(a)], the observable  $J_j'$  is  $J_\pm'$ . Then, the operator can be calculated as follows:

$$\begin{aligned} e^{-i\theta J_y'} e^{-i\Omega t J_z'} J_\pm' e^{i\Omega t J_z'} e^{i\theta J_y'} \\ = e^{-i\theta J_y'} e^{-i\Omega t J_z'} (J_x' \pm iJ_y') e^{i\Omega t J_z'} e^{i\theta J_y'} \\ = e^{-i\theta J_y'} [(J_x' \cos \Omega t + J_y' \sin \Omega t) \\ \pm i(-J_x' \sin \Omega t + J_y' \cos \Omega t)] e^{i\theta J_y'} \\ = e^{-i\theta J_y'} [(J_x' e^{\mp \Omega t} + J_y' e^{\mp(\Omega t - \pi/2)})] e^{i\theta J_y'} \\ = e^{-i\theta J_y'} [(J_x' e^{\mp \Omega t} \pm iJ_y' e^{\mp \Omega t})] e^{i\theta J_y'} \\ = e^{\mp \Omega t} (e^{-i\theta J_y'} J_\pm' e^{i\theta J_y'}). \end{aligned} \quad (7)$$

The expected values are given by

$$\begin{aligned} \langle 3/2; t | e^{-i\theta J_y'} e^{-i\Omega t J_z'} J_+' e^{i\Omega t J_z'} e^{i\theta J_y'} | 1/2; t \rangle \\ = e^{i\omega_Q t} e^{-i\Omega t} \langle 3/2; 0 | e^{-i\theta J_y'} J_+' e^{i\theta J_y'} | 1/2; 0 \rangle, \end{aligned} \quad (8a)$$

$$\begin{aligned} \langle -3/2; t | e^{-i\theta J_y'} e^{-i\Omega t J_z'} J_-' e^{i\Omega t J_z'} e^{i\theta J_y'} | -1/2; t \rangle \\ = e^{i\omega_Q t} e^{i\Omega t} \langle -3/2; 0 | e^{-i\theta J_y'} J_-' e^{i\theta J_y'} | -1/2; 0 \rangle. \end{aligned} \quad (8b)$$

This result indicates that, in the case of transverse coil rotation, the NQR signal splits into two lines with an NQR shift of  $\pm\Omega/2\pi$  and a center frequency of  $\omega_Q/2\pi$ . These NQR intensities can be calculated from the transition probability as follows:

$$| \langle 3/2; 0 | J_+ | 1/2; 0 \rangle |^2 = 3/4, \quad (9a)$$

$$| \langle -3/2; 0 | J_- | -1/2; 0 \rangle |^2 = 3/4. \quad (9b)$$

The NQR intensities of the two lines are equal. These calculations satisfactorily reproduce the observed NQR spectra shown in Fig. 2(a). The rotational Doppler effect arises from the noncommutative property of  $J_\pm'$  and  $e^{\pm i\Omega t J_z'}$  for the transverse coil rotation as expressed in Eq. (7). It should be noted here that the transition probability was calculated using  $J_\pm'$  (not  $J_\pm$ ), whose quantization axis is along the principal axis of the EFG [Fig. 5(a)].

## B. Simultaneous sample and sample coil rotation

We describe the NQR line splittings due to the Barnett field shown in Figs. 3(a) and 3(b) in the following. In addition to the EFG, when the Barnett field acted on the nuclei, the two degenerate spin states of  $|\pm 3/2\rangle$  and  $|\pm 1/2\rangle$  split into four spin states, as shown in Fig. 5(b). In the present case,  $\mathcal{H}_\Omega$  of the Zeeman interaction due to the Barnett field is much weaker than  $\mathcal{H}_Q$  of the quadrupole interaction. Thus, the eigenstate can be obtained by treating  $\mathcal{H}_\Omega$  as a perturbation term [37]. As the Barnett field emerges along the rotation axis,  $\mathcal{H}_\Omega$  can be written as follows:

$$\mathcal{H}_\Omega = -\gamma \hbar B_\Omega (J_z \cos \theta + J_x \sin \theta), \quad (10)$$

where  $\theta$  denotes the angle between the rotation axis and the principal axis of the EFG. In this formula, the quantization axis is along the principal axis of the EFG, and thus,  $J_z$  is also along the principal axis of the EFG. For  $J = 3/2$ , the matrix elements of  $\mathcal{H}_\Omega$  can be written as

$$-\frac{\hbar\Omega}{2} \begin{pmatrix} \sqrt{3} & & & \\ & \sqrt{1/3} & 2\sqrt{2/3} & \\ & 2\sqrt{2/3} & -\sqrt{1/3} & \\ & & & -\sqrt{3} \end{pmatrix}, \quad (11)$$

where the columns and the rows are in the order of  $|3/2\rangle$ ,  $|1/2\rangle$ ,  $|-1/2\rangle$ , and  $|-3/2\rangle$ . There is no coupling between the states of  $\pm 3/2$  and  $\pm 1/2$  because  $\mathcal{H}_\Omega$  is treated as a perturbation, that is,  $\mathcal{H}_\Omega \ll \mathcal{H}_Q$ . The  $\pm 1/2$  block is diagonalized using an unitary operator as follows:

$$R(\alpha) \mathcal{H}_\Omega R(-\alpha) = -\frac{\sqrt{3}\hbar\Omega}{2} \begin{pmatrix} 1 & & & \\ & 1 & & \\ & & -1 & \\ & & & -1 \end{pmatrix}. \quad (12)$$

Here  $R(\alpha)$  is expressed as follows:

$$\begin{aligned} R(\alpha) = \begin{pmatrix} 1 & & & \\ & \cos \alpha & \sin \alpha & \\ & -\sin \alpha & \cos \alpha & \\ & & & 1 \end{pmatrix}, \\ \cos \alpha = \sqrt{2/3}, \quad \sin \alpha = \sqrt{1/3}. \end{aligned} \quad (13)$$

The eigenvectors of the diagonalized  $\mathcal{H}_\Omega$  are in the order of  $|3/2\rangle$ ,  $|+\rangle$ ,  $|-\rangle$ , and  $|-3/2\rangle$ , where  $|+\rangle$  and  $|-\rangle$  are expressed as  $|+\rangle = \sqrt{2/3}|1/2\rangle + \sqrt{1/3}|-1/2\rangle$  and  $|-\rangle = -\sqrt{1/3}|1/2\rangle + \sqrt{2/3}|-1/2\rangle$ . Then, the single transition splits into four as  $|+3/2\rangle \leftrightarrow |+\rangle$ ,  $|+3/2\rangle \leftrightarrow |-\rangle$ ,  $|-3/2\rangle \leftrightarrow |+\rangle$ , and  $|-3/2\rangle \leftrightarrow |-\rangle$ .

The time evolution of the nuclear spin states can be written as

$$|k; t\rangle = e^{J_0' dt' \mathcal{H}_Q / \hbar} e^{J_0' dt' \mathcal{H}_\Omega / \hbar} |k; 0\rangle. \quad (14)$$

We also define the operator for the Barnett field as

$$e^{-i\theta J_y'} J_j' e^{i\theta J_y'}. \quad (15)$$

Compared with Eq. (3), the  $e^{\pm i\Omega t J_z'}$  operator is absent owing to the lack of relative rotation between the sample and sample coil. Instead of the  $e^{\pm i\Omega t J_z'}$  operator, the rotation effect is reflected in the Barnett field. The general formula for the

expected value of the time-dependent spin state for a Barnett field can be expressed as

$$\begin{aligned}
 & \langle k'; t | e^{-i\theta J'_y} J'_z e^{i\theta J'_y} | k; t \rangle \\
 &= \langle k'; 0 | e^{-\int_0^t dt' \mathcal{H}_\Omega / i\hbar} e^{-\int_0^t dt' \mathcal{H}_Q / i\hbar} e^{-i\theta J'_y} J'_z e^{i\theta J'_y} \\
 & \quad \times e^{\int_0^t dt' \mathcal{H}_Q / i\hbar} e^{\int_0^t dt' \mathcal{H}_\Omega / i\hbar} | k; 0 \rangle \\
 &= e^{-(E_Q^k - E_Q^k) t / i\hbar} e^{-(E_\Omega^k - E_\Omega^k) t / i\hbar} \langle k'; 0 | e^{-i\theta J'_y} J'_z e^{i\theta J'_y} | k; 0 \rangle. \quad (16)
 \end{aligned}$$

In the case of the longitudinal coil shown in Fig. 3(b), the observable  $J'_j$  is  $J'_z$ . Then, the expected values are given by

$$\begin{aligned}
 & \langle 3/2; t | e^{-i\theta J'_y} J'_z e^{i\theta J'_y} | +; t \rangle \\
 &= e^{i\omega_Q t} \langle 3/2; 0 | e^{-i\theta J'_y} J'_z e^{i\theta J'_y} | +; 0 \rangle, \quad (17a)
 \end{aligned}$$

$$\begin{aligned}
 & \langle 3/2; t | e^{-i\theta J'_y} J'_z e^{i\theta J'_y} | -; t \rangle \\
 &= e^{i\omega_Q t} e^{-i\sqrt{3}\Omega t} \langle 3/2; 0 | e^{-i\theta J'_y} J'_z e^{i\theta J'_y} | -; 0 \rangle, \quad (17b)
 \end{aligned}$$

$$\begin{aligned}
 & \langle -3/2; t | e^{-i\theta J'_y} J'_z e^{i\theta J'_y} | +; t \rangle \\
 &= e^{i\omega_Q t} e^{i\sqrt{3}\Omega t} \langle -3/2; 0 | e^{-i\theta J'_y} J'_z e^{i\theta J'_y} | +; 0 \rangle, \quad (17c)
 \end{aligned}$$

$$\begin{aligned}
 & \langle -3/2; t | e^{-i\theta J'_y} J'_z e^{i\theta J'_y} | -; t \rangle \\
 &= e^{i\omega_Q t} \langle -3/2; 0 | e^{-i\theta J'_y} J'_z e^{i\theta J'_y} | -; 0 \rangle. \quad (17d)
 \end{aligned}$$

This result indicates that, in the case of longitudinal coil rotation, the NQR signal splits into three lines with a shift of  $\pm\sqrt{3}\Omega/2\pi$  and a center frequency of  $\omega_Q/2\pi$ . The transition probability can be written as

$$| \langle 3/2; 0 | J_+ | +; 0 \rangle |^2 = 1/2, \quad (18a)$$

$$| \langle 3/2; 0 | J_+ | -; 0 \rangle |^2 = 1/4, \quad (18b)$$

$$| \langle -3/2; 0 | J_- | +; 0 \rangle |^2 = 1/4, \quad (18c)$$

$$| \langle -3/2; 0 | J_- | -; 0 \rangle |^2 = 1/2. \quad (18d)$$

The ratio of the NQR intensities with the frequencies  $(-\sqrt{3}\Omega + \omega_Q)/2\pi$ ,  $\omega_Q/2\pi$ , and  $(\sqrt{3}\Omega + \omega_Q)/2\pi$  is 1:4:1. The results satisfactorily reproduce the observed NQR spectra shown in Fig. 3(b).

In the case of the transverse coil shown in Fig. 3(a), the observable  $J'_j$  is  $J'_\pm$ . Then, the expected values are given by

$$\begin{aligned}
 & \langle 3/2; t | e^{-i\theta J'_y} J'_+ e^{i\theta J'_y} | +; t \rangle \\
 &= e^{i\omega_Q t} \langle 3/2; 0 | e^{-i\theta J'_y} J'_+ e^{i\theta J'_y} | +; 0 \rangle, \quad (19a)
 \end{aligned}$$

$$\begin{aligned}
 & \langle 3/2; t | e^{-i\theta J'_y} J'_+ e^{i\theta J'_y} | -; t \rangle \\
 &= e^{i\omega_Q t} e^{-i\sqrt{3}\Omega t} \langle 3/2; 0 | e^{-i\theta J'_y} J'_+ e^{i\theta J'_y} | -; 0 \rangle, \quad (19b)
 \end{aligned}$$

$$\begin{aligned}
 & \langle -3/2; t | e^{-i\theta J'_y} J'_- e^{i\theta J'_y} | +; t \rangle \\
 &= e^{i\omega_Q t} e^{i\sqrt{3}\Omega t} \langle -3/2; 0 | e^{-i\theta J'_y} J'_- e^{i\theta J'_y} | +; 0 \rangle, \quad (19c)
 \end{aligned}$$

$$\begin{aligned}
 & \langle -3/2; t | e^{-i\theta J'_y} J'_- e^{i\theta J'_y} | -; t \rangle \\
 &= e^{i\omega_Q t} \langle -3/2; 0 | e^{-i\theta J'_y} J'_- e^{i\theta J'_y} | -; 0 \rangle. \quad (19d)
 \end{aligned}$$

The result indicates that, in the case of transverse coil rotation, the NQR signal also splits into three lines with an NQR shift of  $\pm\sqrt{3}\Omega/2\pi$  and a center frequency of  $\omega_Q/2\pi$ . The transition probability is given by Eqs. (18a)–(18d). The

ratio of the NQR intensities with frequencies of  $(-\sqrt{3}\Omega + \omega_Q)/2\pi$ ,  $\omega_Q/2\pi$ , and  $(\sqrt{3}\Omega + \omega_Q)/2\pi$  is 1:4:1. The results reproduce the observed NQR spectra shown in Fig. 3(a).

As shown in Figs. 3(a) and 3(b), the two sets of observed NQR spectra were identical. The reason for this is the absence of the rotational Doppler effects owing to the lack of relative rotation between the sample and sample coil.

### C. Only sample rotation

We formulate the NQR spectra shown in Figs. 4(a) and 4(b) in the following. The structures of the NQR spectra can be explained in two ways. The first involves the combination of the Barnett field and the rotational Doppler effect. In this case, we first consider the NQR spectra due to the Barnett field in the rotating frame of reference and then consider the NQR spectra in the laboratory frame of reference, taking into account the rotational Doppler effect due to the relative rotation. The other involves the Berry phase. In this case, we directly observe the spin dynamics in the rotating sample from the laboratory frame of reference.

#### 1. Barnett field and rotational Doppler effect

First, we consider the Barnett field in the same rotating frame of reference as the sample. The NQR line splits into three lines owing to the Barnett field, as shown in Figs. 3(a) and 3(b). Then, we apply the rotational Doppler effect for each resonance frequency. The time evolution of the nuclear spin states is given by Eq. (14). The operator of the rotational Doppler effect is as follows:

$$e^{-i\theta J'_y} e^{i\Omega t J'_z} J'_j e^{-i\Omega t J'_z} e^{i\theta J'_y}. \quad (20)$$

Here note that the sign of  $i\Omega t J'_z$  is opposite that in Eq. (3). This difference arises from the difference in the direction of relative rotation; Eq. (3) expresses the rotation of the sample coil, whereas Eq. (20) expresses the rotation of the sample itself. The general formula for the expected value of the time-dependent spin state for the combination of the Barnett field and the rotational Doppler effect can be written as

$$\begin{aligned}
 & \langle k'; t | e^{-i\theta J'_y} e^{i\Omega t J'_z} J'_j e^{-i\Omega t J'_z} e^{i\theta J'_y} | k; t \rangle \\
 &= \langle k'; 0 | e^{-\int_0^t dt' \mathcal{H}_\Omega / i\hbar} e^{-\int_0^t dt' \mathcal{H}_Q / i\hbar} e^{-i\theta J'_y} e^{i\Omega t J'_z} J'_j e^{-i\Omega t J'_z} e^{i\theta J'_y} \\
 & \quad \times e^{\int_0^t dt' \mathcal{H}_Q / i\hbar} e^{\int_0^t dt' \mathcal{H}_\Omega / i\hbar} | k; 0 \rangle \\
 &= e^{-(E_Q^k - E_Q^k) t / i\hbar} e^{-(E_\Omega^k - E_\Omega^k) t / i\hbar} \langle k'; 0 | e^{-i\theta J'_y} e^{i\Omega t J'_z} J'_j \\
 & \quad \times e^{-i\Omega t J'_z} e^{i\theta J'_y} | k; 0 \rangle. \quad (21)
 \end{aligned}$$

In the case of the longitudinal coil shown in Fig. 4(b), the observable  $J'_j$  is  $J'_z$ . Then, the operator is calculated:

$$e^{-i\theta J'_y} e^{i\Omega t J'_z} J'_z e^{-i\Omega t J'_z} e^{i\theta J'_y} = e^{-i\theta J'_y} J'_z e^{i\theta J'_y}. \quad (22)$$

The expected values are given by Eqs. (17a)–(17d). This result indicates that, in the case of the longitudinal coil, the NQR signal splits into three lines with an NQR shift of  $\pm\sqrt{3}\Omega/2\pi$  and a center frequency of  $\omega_Q/2\pi$ . The transition probability is given by Eqs. (18a)–(18d). The ratio of the NQR intensities with frequencies of  $(-\sqrt{3}\Omega + \omega_Q)/2\pi$ ,  $\omega_Q/2\pi$ , and  $(\sqrt{3}\Omega +$

$\omega_Q)/2\pi$  is 1:4:1. This calculation satisfactorily reproduces the observed NQR spectra as shown in Fig. 4(b).

In the case of the transverse coil shown in Fig. 4(a), the observable  $J'_y$  is  $J'_\pm$ . Then, the operators can be calculated as

$$e^{-i\theta J'_y} e^{i\Omega t J'_z} J'_\pm e^{-i\Omega t J'_z} e^{i\theta J'_y} = e^{\pm i\Omega t} (e^{-i\theta J'_y} J'_\pm e^{i\theta J'_y}). \quad (23)$$

The expected values are given by

$$\begin{aligned} & \langle 3/2; t | e^{-i\theta J'_y} e^{i\Omega t J'_z} J'_+ e^{-i\Omega t J'_z} e^{i\theta J'_y} | +; t \rangle \\ &= e^{i\omega_Q t} e^{i\Omega t} \langle 3/2; 0 | e^{-i\theta J'_y} J'_+ e^{i\theta J'_y} | +; 0 \rangle, \end{aligned} \quad (24a)$$

$$\begin{aligned} & \langle 3/2; t | e^{-i\theta J'_y} e^{i\Omega t J'_z} J'_+ e^{-i\Omega t J'_z} e^{i\theta J'_y} | -; t \rangle \\ &= e^{i\omega_Q t} e^{-i\sqrt{3}\Omega t} e^{i\Omega t} \langle 3/2; 0 | e^{-i\theta J'_y} J'_+ e^{i\theta J'_y} | -; 0 \rangle, \end{aligned} \quad (24b)$$

$$\begin{aligned} & \langle -3/2; t | e^{-i\theta J'_y} e^{i\Omega t J'_z} J'_- e^{-i\Omega t J'_z} e^{i\theta J'_y} | +; t \rangle \\ &= e^{i\omega_Q t} e^{i\sqrt{3}\Omega t} e^{-i\Omega t} \langle -3/2; 0 | e^{-i\theta J'_y} J'_- e^{i\theta J'_y} | +; 0 \rangle, \end{aligned} \quad (24c)$$

$$\begin{aligned} & \langle -3/2; t | e^{-i\theta J'_y} e^{i\Omega t J'_z} J'_- e^{-i\Omega t J'_z} e^{i\theta J'_y} | -; t \rangle \\ &= e^{i\omega_Q t} e^{-i\Omega t} \langle -3/2; 0 | e^{-i\theta J'_y} J'_- e^{i\theta J'_y} | -; 0 \rangle. \end{aligned} \quad (24d)$$

This result indicates that, in the case of the transverse coil, the NQR signal splits into four lines with NQR shifts of  $[\pm(\sqrt{3}-1)\Omega]/2\pi$  and  $\pm\Omega/2\pi$ . The transition probability is given by Eqs. (18a)–(18d). The ratio of the NQR intensities with frequencies of  $(\Omega + \omega_Q)/2\pi$ ,  $[(\sqrt{3}-1)\Omega + \omega_Q]/2\pi$ ,  $[-(\sqrt{3}-1)\Omega + \omega_Q]/2\pi$ , and  $(-\Omega + \omega_Q)/2\pi$  is 2:1:1:2. This calculation satisfactorily reproduces the observed NQR spectra shown in Fig. 4(a). The NQR shifts expressed in Eqs. (24a)–(24d) are simulated in Fig. 5(c). The upper NQR spectrum in Fig. 5(c) represents line splitting due to the Barnett field expressed in Eqs. (17a)–(17d). The lower NQR spectrum in Fig. 5(c) is the resulting NQR spectrum after including the rotational Doppler effect [Eqs. (24a)–(24d)].

## 2. Berry phase

First, we provide a description of the Berry phase for the experimental results shown in Figs. 4(a) and 4(b). In the setup shown in Fig. 4, the nuclear precession in the rotating sample is observed by an observer in the laboratory frame of reference. In this case, the principal axis of the EFG is rotating. This means that the quantization axis of the nuclear spin system is also rotating. In this situation, a cyclic time-dependent Hamiltonian should be resolved. In an adiabatic limit, in which the rotational frequency is much less than that of the EFG, that is,  $\omega_Q \gg \Omega$ , the Hamiltonian can be approximately reduced by introducing the Berry phase [11, 38].

We consider the time-dependent Hamiltonian  $\mathcal{H}_Q(t)$  as follows:

$$\begin{aligned} \langle k'; 0 | \mathcal{H}_Q | k; 0 \rangle &= \langle k'; 0 | U U^\dagger \mathcal{H}_Q U U^\dagger | k; 0 \rangle \\ &= \langle k'; t | \mathcal{H}_Q(t) | k; t \rangle. \end{aligned} \quad (25)$$

Here  $U = e^{-i\theta J'_y} e^{i\Omega t J'_z}$ . Then,  $|k; t\rangle = e^{-i\Omega t J'_z} e^{i\theta J'_y} |k; 0\rangle$  means that the spin state is tilted from the  $z$  axis by  $\theta$  and rotates about the  $z$  axis with frequency  $\Omega/2\pi$ . According to the Berry description, the spin state can be written as follows:

$$e^{i\gamma_k} e^{i \int^t ds \mathcal{H}_Q / \hbar} |k; t\rangle, \quad (26)$$

where  $\gamma_k$  is the Berry phase and its accumulation is written as

$$\begin{aligned} \gamma_{k'k} &= i \int_0^t dt' \langle k'; t' | \frac{\partial}{\partial t'} | k; t' \rangle \\ &= i \int_0^t dt' \langle k'; 0 | e^{-i\theta J'_y} e^{i\Omega t' J'_z} \frac{\partial}{\partial t'} e^{-i\Omega t' J'_z} e^{i\theta J'_y} | k; 0 \rangle \\ &= \int_0^t dt' \langle k'; 0 | e^{-i\theta J'_y} e^{i\Omega t' J'_z} (\Omega J'_z) e^{-i\Omega t' J'_z} e^{i\theta J'_y} | k; 0 \rangle \\ &= \Omega t \langle k'; 0 | e^{-i\theta J'_y} J'_z e^{i\theta J'_y} | k; 0 \rangle \\ &= \Omega t \langle k'; 0 | (J'_z \cos \theta + J'_x \sin \theta) | k; 0 \rangle. \end{aligned} \quad (27)$$

Then, the matrix element can be expressed as

$$\frac{\Omega t}{2} \begin{pmatrix} \sqrt{3} & & & \\ & \sqrt{1/3} & 2\sqrt{2/3} & \\ & 2\sqrt{2/3} & -\sqrt{1/3} & \\ & & & -\sqrt{3} \end{pmatrix}, \quad (28)$$

where the columns and the rows are in the order of  $|3/2\rangle$ ,  $|1/2\rangle$ ,  $|-1/2\rangle$ , and  $|-3/2\rangle$ . There is no coupling between the states of  $\pm 3/2$  and  $\pm 1/2$  owing to the adiabatic limit  $\omega_Q \gg \Omega$ . The  $\pm 1/2$  block is diagonalized using the unitary operator defined in Eq. (13) as follows:

$$\frac{\sqrt{3}\Omega t}{2} \begin{pmatrix} 1 & & & \\ & 1 & & \\ & & -1 & \\ & & & -1 \end{pmatrix}. \quad (29)$$

The eigenvectors of the diagonalized  $\gamma_{k'k}$  are in the order of  $|3/2\rangle$ ,  $|+\rangle$ ,  $|-\rangle$ , and  $|-3/2\rangle$ .

The general formula for Berry's description of the time-dependent spin state is given by

$$\begin{aligned} & \langle k'; t | e^{-\int^t dt' \mathcal{H}_Q / \hbar} e^{-i\gamma_k} J'_y e^{i\gamma_k} e^{\int^t dt' \mathcal{H}_Q / \hbar} | k; t \rangle \\ &= \langle k'; 0 | e^{-i\theta J'_y} e^{i\Omega t J'_z} e^{-\int^t dt' \mathcal{H}_Q / \hbar} e^{-i\gamma_k} J'_y e^{i\gamma_k} e^{\int^t dt' \mathcal{H}_Q / \hbar} \\ &\quad \times e^{-i\Omega t J'_z} e^{i\theta J'_y} | k; 0 \rangle \\ &= e^{-i(\gamma_k - \gamma_k)} e^{-(E_Q^k - E_Q^k) t / \hbar} \langle k'; 0 | e^{-i\theta J'_y} e^{i\Omega t J'_z} J'_y \\ &\quad \times e^{-i\Omega t J'_z} e^{i\theta J'_y} | k; 0 \rangle. \end{aligned} \quad (30)$$

In the case of the longitudinal coil shown in Fig. 4(b), the observable  $J'_y$  is  $J'_z$ . Then, the operator is calculated as

$$e^{-i\theta J'_y} e^{i\Omega t J'_z} J'_z e^{-i\Omega t J'_z} e^{i\theta J'_y} = e^{-i\theta J'_y} J'_z e^{i\theta J'_y}. \quad (31)$$

The expected values are written as

$$\begin{aligned} & \langle 3/2; t | e^{-\int^t dt' \mathcal{H}_Q / \hbar} e^{-i\gamma_k} J'_z e^{i\gamma_k} e^{\int^t dt' \mathcal{H}_Q / \hbar} | +; t \rangle \\ &= e^{i\omega_Q t} \langle 3/2; 0 | e^{-i\theta J'_y} J'_z e^{i\theta J'_y} | +; 0 \rangle, \end{aligned} \quad (32a)$$

$$\begin{aligned} & \langle 3/2; t | e^{-\int^t dt' \mathcal{H}_Q / \hbar} e^{-i\gamma_k} J'_z e^{i\gamma_k} e^{\int^t dt' \mathcal{H}_Q / \hbar} | -; t \rangle \\ &= e^{i\omega_Q t} e^{-i\sqrt{3}\Omega t} \langle 3/2; 0 | e^{-i\theta J'_y} J'_z e^{i\theta J'_y} | -; 0 \rangle, \end{aligned} \quad (32b)$$

$$\begin{aligned} & \langle -3/2; t | e^{-\int^t dt' \mathcal{H}_Q / \hbar} e^{-i\gamma_k} J'_z e^{i\gamma_k} e^{\int^t dt' \mathcal{H}_Q / \hbar} | +; t \rangle \\ &= e^{i\omega_Q t} e^{i\sqrt{3}\Omega t} \langle -3/2; 0 | e^{-i\theta J'_y} J'_z e^{i\theta J'_y} | +; 0 \rangle, \end{aligned} \quad (32c)$$

$$\begin{aligned} & \langle -3/2; t | e^{-\int^t dt' \mathcal{H}_Q / \hbar} e^{-i\gamma_k} J'_z e^{i\gamma_k} e^{\int^t dt' \mathcal{H}_Q / \hbar} | -; t \rangle \\ &= e^{i\omega_Q t} \langle -3/2; 0 | e^{-i\theta J'_y} J'_z e^{i\theta J'_y} | -; 0 \rangle. \end{aligned} \quad (32d)$$

This result indicates that, in the case of the longitudinal coil rotation, the NQR signal also splits into three lines with an NQR shift of  $\pm\sqrt{3}\Omega/2\pi$  and a center frequency  $\omega_Q/2\pi$ . The transition probability is given by Eqs. (18a)–(18d). The ratio of the NQR intensities with frequencies of  $(-\sqrt{3}\Omega + \omega_Q)/2\pi$ ,  $\omega_Q/2\pi$ , and  $(\sqrt{3}\Omega + \omega_Q)/2\pi$  is 1:4:1. The result satisfactorily reproduces the NQR spectra shown in Fig. 4(b).

In the case of transverse coil rotation as shown in Fig. 4(a), the observable  $J_j$  is  $J_{\pm}$ . Then, the expected values are given by

$$\begin{aligned} \langle 3/2; t | e^{-\int^t dt' \mathcal{H}_Q/i\hbar} e^{-i\gamma_k t'} J'_+ e^{i\gamma_k t'} e^{\int^t dt' \mathcal{H}_Q/i\hbar} | +; t \rangle \\ = e^{i\omega_Q t} e^{i\Omega t} \langle 3/2; 0 | e^{-i\theta J'_y} J'_+ e^{i\theta J'_y} | +; 0 \rangle, \end{aligned} \quad (33a)$$

$$\begin{aligned} \langle 3/2; t | e^{-\int^t dt' \mathcal{H}_Q/i\hbar} e^{-i\gamma_{k'}} J'_+ e^{i\gamma_k t'} e^{\int^t dt' \mathcal{H}_Q/i\hbar} | -; t \rangle \\ = e^{i\omega_Q t} e^{-i\sqrt{3}\Omega t} e^{i\Omega t} \langle 3/2; 0 | e^{-i\theta J'_y} J'_+ e^{i\theta J'_y} | -; 0 \rangle, \end{aligned} \quad (33b)$$

$$\begin{aligned} \langle -3/2; t | e^{-\int^t dt' \mathcal{H}_Q/i\hbar} e^{-i\gamma_{k'}} J'_- e^{i\gamma_k t'} e^{\int^t dt' \mathcal{H}_Q/i\hbar} | +; t \rangle \\ = e^{i\omega_Q t} e^{i\sqrt{3}\Omega t} e^{-i\Omega t} \langle -3/2; 0 | e^{-i\theta J'_y} J'_- e^{i\theta J'_y} | +; 0 \rangle, \end{aligned} \quad (33c)$$

$$\begin{aligned} \langle -3/2; t | e^{-\int^t dt' \mathcal{H}_Q/i\hbar} e^{-i\gamma_{k'}} J'_- e^{i\gamma_k t'} e^{\int^t dt' \mathcal{H}_Q/i\hbar} | -; t \rangle \\ = e^{i\omega_Q t} e^{-i\Omega t} \langle -3/2; 0 | e^{-i\theta J'_y} J'_- e^{i\theta J'_y} | -; 0 \rangle. \end{aligned} \quad (33d)$$

This result indicates that, in the case of transverse coil rotation, the NQR signal splits into four lines with NQR shifts of  $\pm(\sqrt{3}-1)\Omega/2\pi$  and  $\pm\Omega/2\pi$ . The transition probability is given by Eqs. (18a)–(18d). The ratio of the NQR intensities with frequencies of  $(\Omega + \omega_Q)/2\pi$ ,  $[(\sqrt{3}-1)\Omega + \omega_Q]/2\pi$ ,  $[-(\sqrt{3}-1)\Omega + \omega_Q]/2\pi$ , and  $(-\Omega + \omega_Q)/2\pi$  is 2:1:1:2. This result satisfactorily reproduces the observed NQR spectra shown in Fig. 4(a). The NQR shifts expressed in Eqs. (33a)–(33d) are simulated in Fig. 5(c). The upper NQR spectrum in Fig. 5(c) represents line splitting due to the Berry phase expressed in Eqs. (32a)–(32d). The lower NQR spectrum in Fig. 5(c) is the resulting NQR spectrum after including the rotational Doppler effect [Eqs. (33a)–(33d)].

## V. DISCUSSION

As shown in Figs. 2(a), 2(b), 3(a), and 3(b), the NQR spectra obtained under simultaneous sample and sample coil rotation were completely different from those recorded under only coil rotation. This finding demonstrates that the rotational Doppler effect and the Barnett field are distinct phenomena. Under the setup with simultaneous rotation of the sample and sample coil, the NQR spectra split into three lines and could be simply explained by introducing the Barnett field into the rotating frame. This was also the case for the NQR spectra obtained using the longitudinal and transverse coils. The reason for this is that there is no relative rotation between the sample and sample coil; thus, the time-dependent operator  $e^{\pm i\Omega t J'_z}$  is not necessary.

In contrast, as shown in Figs. 2(a) and 2(b), under the setup with only transverse coil rotation, the NQR spectra split into two lines, whereas under longitudinal coil rotation the NQR spectra did not change. This difference arises from the noncommutative property of  $J'_z$  and  $e^{i\Omega t J'_z}$  for transverse coil rotation and the commutative property of  $J'_z$  and  $e^{i\Omega t J'_z}$  for longitudinal coil rotation. It should be noted that longitudinal coil

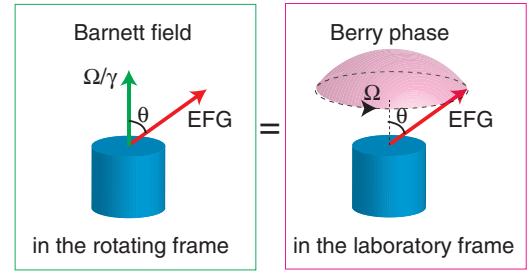


FIG. 6. Illustration of the equivalence of the Barnett field and the Berry phase.

rotation, in which the coil axis is parallel to the rotation axis, does not cause the rotational Doppler effect. Consequently, the coupling between the coupling coil and the stationary coil, which transmits the NQR signal from the rotating frame to the laboratory frame, does not cause rotational Doppler effects because both the coupling coil and stationary coil are parallel to the rotation axis.

In the case of only sample rotation, as shown in Figs. 4(a) and 4(b), we have provided two explanations. The first is based on the combination of the Barnett field in the rotating frame and the rotational Doppler effect and the second involves the Berry phase. Both explanations account for the observed NQR spectra shown in Figs. 4(a) and 4(b) owing to the equivalence of the Barnett field and the Berry phase accumulation, that is,  $e^{-(E_{\Omega}^k - E_{\Omega}^k)t/i\hbar} = e^{-i(\gamma_{k'} - \gamma_k)t}$ , as shown in Eqs. (21) and (30). The cause of this is the identical matrix elements due to the equivalence of the perturbation of the Barnett field in the rotating frame and the Berry phase accumulation in the adiabatic limit in the laboratory frame, as shown in Eqs. (11) and (28). This relation is illustrated in Fig. 6. The Barnett field and the Berry phase can be regarded as a gauge field in the rotating frame and the laboratory frame, respectively [35]. The difference in the NQR spectra between Figs. 4(a) and 4(b) arises from the rotational Doppler effect, which appears in only the case of the transverse coil. The relation between the Barnett field, the rotational Doppler effect, and the Berry phase effect is summarized in Table I.

According to our previous reports describing the NMR detection of Barnett fields [25], the NMR lines shift by the same frequency as the rotational frequency  $\Omega/2\pi$  under simultaneous rotation of the sample and sample coil. Because in this setup the rotation axis is parallel to the external field, there is no accumulation of the Berry phase. The NMR shift originates from the Barnett field due to sample rotation. This interpretation is consistent with the present NQR results shown in Fig. 3(a). Under only sample coil rotation [26], the NMR lines also shift by the same frequency as the rotational frequency  $\Omega/2\pi$ . As the sample is stationary in this setup, no Barnett field acts upon it. Therefore, the NMR shift arises from the rotational Doppler effect. This interpretation is consistent with the present results shown in Fig. 2(a). Although the two setups provide NMR shifts of the same magnitude, they result in different NQR line splittings. These results indicate that the case of simultaneous sample and sample coil rotation is fundamentally different from that of only sample coil rotation. In the case of only sample rotation, the Barnett field and rotational Doppler effect cancel each other out, resulting in no NMR



TABLE I. Variation of the physical phenomena arising from rotation depending on the experimental setup.

Setup	Coil $\parallel \Omega$	Coil $\perp \Omega$
Only coil rotation		Rotational Doppler effect
Sample and sample coil rotation	Barnett field	Barnett field
Only sample rotation	Barnett field = Berry phase	Barnett field + rotational Doppler effect = Berry phase + rotational Doppler effect

shift. As shown by the present NQR experiments, the forms of the Hamiltonians are different between the quadrupole and the Barnett field terms, which generates different NQR shifts, resulting in no cancellation of the Barnett field and rotational Doppler effects even in the setup involving only sample rotation. Thus, the criticism in Ref. [34] that the NMR shifts observed for only coil rotation and simultaneous sample and sample coil rotation can be explained solely by the sample coil rotation and therefore that rotating the sample is not essential is demonstrated to be irrelevant.

## VI. CONCLUSION

In conclusion, we have evaluated the role of the rotational Doppler effect, Barnett field, and Berry phase in NQR measurements under three setups: only sample coil rotation, simultaneous sample and sample coil rotation, only sample rotation. We have experimentally shown the difference between the Barnett field and the rotational Doppler effect and

the equivalence of the Barnett field in the rotating frame and the Berry phase in the laboratory frame. We have also experimentally confirmed the existence of the Barnett field and the rotational Doppler effect. The results indicate that, when describing the effects of mechanical rotation on magnetic resonance measurements such as NMR and NQR, one should simultaneously take into consideration the Barnett field, the rotational Doppler effect, and the Berry phase.

## ACKNOWLEDGMENTS

The authors thank H. Yasuoka, K. Harii, M. Sato, Y. Ohnuma, and J. Ieda for valuable discussions, Y. Haga for the x-ray diffraction experiment, and M. Ono for technical support. This work was financially supported by JST ERATO ‘‘Spin Quantum Rectification Project’’ (Grant No. JPMJER1402), JST CREST (Grants No. JPMJCR19J4, No. JPMJCR1874, No. JPMJCR20C1 and No. JPMJCR20T2), and JSPS KAKENHI (Grants No. JP19H05600, No. JP17H02927, No. JP20H01863, No. JP20H01865 and No. JP21H01800).

- [1] A. Einstein and W. J. de Haas, *Proc. K. Ned. Akad. Wet.* **18 I**, 696 (1915).
- [2] S. J. Barnett, *Phys. Rev.* **6**, 239 (1915).
- [3] S. J. Barnett, *Rev. Mod. Phys.* **7**, 129 (1935).
- [4] G. G. Scott, *Rev. Mod. Phys.* **34**, 102 (1962).
- [5] R. Huguenin and D. Baldock, *Phys. Rev. Lett.* **16**, 795 (1966).
- [6] R. Huguenin, G. P. Pells, and D. N. Baldock, *J. Phys. F* **1**, 281 (1971).
- [7] M. V. Berry, *Proc. R. Soc. London, Ser. A* **392**, 45 (1984).
- [8] Y. Aharonov and J. Anandan, *Phys. Rev. Lett.* **58**, 1593 (1987).
- [9] S. Appelt, G. Wackerle, and M. Mehring, *Phys. Rev. Lett.* **72**, 3921 (1994).
- [10] S. Appelt, G. Wackerle, and M. Mehring, *Z. Phys. D* **34**, 75 (1995).
- [11] R. Tycko, *Phys. Rev. Lett.* **58**, 2281 (1987).
- [12] J. W. Zwanziger, M. Koenig, and A. Pines, *Phys. Rev. A* **42**, 3107 (1990).
- [13] K. Harii, Y.-J. Seo, Y. Tsutsumi, H. Chudo, K. Oyanagi, M. Matsuo, Y. Shiomi, T. Ono, S. Maekawa, and E. Saitoh, *Nat. Commun.* **10**, 2616 (2019).
- [14] T. M. Wallis, J. Moreland, and P. Kabos, *Appl. Phys. Lett.* **89**, 122502 (2006).
- [15] K. Mori, M. G. Dunsmore, J. E. Losby, D. M. Jenson, M. Belov, and M. R. Freeman, *Phys. Rev. B* **102**, 054415 (2020).
- [16] G. Zolfagharkhani, A. Gaidarzhy, P. Degiovanni, S. Kettemann, P. Fulde, and P. Mohanty, *Nat. Nanotechnol.* **3**, 720 (2008).
- [17] R. Takahashi, M. Matsuo, M. Ono, K. Harii, H. Chudo, S. Okayasu, J. Ieda, S. Takahashi, S. Maekawa, and E. Saitoh, *Nat. Phys.* **12**, 52 (2015).
- [18] R. Takahashi, H. Chudo, M. Matsuo, K. Harii, Y. Ohnuma, S. Maekawa, and E. Saitoh, *Nat. Commun.* **11**, 3009 (2020).
- [19] M. Matsuo, E. Saitoh, and S. Maekawa, *J. Phys. Soc. Jpn.* **86**, 011011 (2017).
- [20] H. T. Kazerooni, A. Thieme, J. Schumacher, and C. Cierpka, *Phys. Rev. Appl.* **14**, 014002 (2020).
- [21] D. Kobayashi, T. Yoshikawa, M. Matsuo, R. Iguchi, S. Maekawa, E. Saitoh, and Y. Nozaki, *Phys. Rev. Lett.* **119**, 077202 (2017).
- [22] M. Matsuo, J. Ieda, K. Harii, E. Saitoh, and S. Maekawa, *Phys. Rev. B* **87**, 180402(R) (2013).
- [23] M. Imai, Y. Ogata, H. Chudo, M. Ono, K. Harii, M. Matsuo, Y. Ohnuma, S. Maekawa, and E. Saitoh, *Appl. Phys. Lett.* **113**, 052402 (2018).
- [24] M. Imai, H. Chudo, M. Ono, K. Harii, M. Matsuo, Y. Ohnuma, S. Maekawa, and E. Saitoh, *Appl. Phys. Lett.* **114**, 162402 (2019).
- [25] H. Chudo, M. Ono, K. Harii, M. Matsuo, J. Ieda, R. Haruki, S. Okayasu, S. Maekawa, H. Yasuoka, and E. Saitoh, *Appl. Phys. Express* **7**, 063004 (2014).

- [26] H. Chudo, K. Harii, M. Matsuo, J. Ieda, M. Ono, S. Maekawa, and E. Saitoh, *J. Phys. Soc. Jpn.* **84**, 043601 (2015).
- [27] K. Harii, H. Chudo, M. Ono, M. Matsuo, J. Ieda, S. Okayasu, S. Maekawa, and E. Saitoh, *Jpn. J. Appl. Phys.* **54**, 050302 (2015).
- [28] M. Arabgol and T. Sleator, *Phys. Rev. Lett.* **122**, 177202 (2019).
- [29] J. Fröhlich and U. M. Studer, *Rev. Mod. Phys.* **65**, 733 (1993).
- [30] F. W. Hehl and W. T. Ni, *Phys. Rev. D* **42**, 2045 (1990).
- [31] M. Matsuo, J. Ieda, E. Saitoh, and S. Maekawa, *Phys. Rev. B* **84**, 104410 (2011).
- [32] L. D. Landau and E. M. Lifshitz, *Electrodynamics of Continuous Media*, 2nd ed. (Butterworth Heinemann, Oxford, UK, 1976).
- [33] E. L. Hahn, B. K. Tenn, and M. P. Augustine, in *Novel NMR and EPR Techniques*, Lecture Notes in Physics Vol. 684 (Springer, Berlin, 2006), p. 1.
- [34] J. Jeener, *Appl. Phys. Express* **13**, 109101 (2020).
- [35] H. Chudo, M. Matsuo, K. Harii, M. Maekawa, and E. Saitoh, *Appl. Phys. Express* **13**, 109102 (2020).
- [36] D. Suter, G. C. Chingas, R. A. Harris, and A. Pines, *Mol. Phys.* **61**, 1327 (1987).
- [37] A. Abragam, *The Principles of Nuclear Magnetism* (Oxford University Press, London, 1961).
- [38] A. Bohm, A. Mostafazadeh, H. Koizumi, Q. Niu, and J. Zwanzinger, *The Geometric Phase in Quantum Systems* (Springer, Berlin, 2003).